Environmental Earth Sciences (2025) 84:209
https://doi.org/10.1007/s12665-025-12225-0

ORIGINAL ARTICLE

A geospatial approach to understanding sinkhole formation in Akgöl Wetland, Türkiye

Muhammed Zeynel Öztürk[1] · Murat Poyraz[2] · Hüseyin Duman[3] · Enes Taşoğlu[1]

Received: 28 November 2024 / Accepted: 24 March 2025 / Published online: 7 April 2025

Abstract

The over-extraction of groundwater for agricultural purposes in the Konya Closed Basin (KCB) has led to land subsidence and new cover collapse sinkholes (CCS) in regions like the Akgöl Wetland (AW), where such occurrences were previously absent. InSAR data from 2014 to 2023 indicate that the average annual subsidence in AW varies between 15 mm/year and 30 mm/year. Alarmingly, in specific locations, the cumulative subsidence has reached 230 mm over nine years. The significant subsidence observed in the southern region of the study area aligns with a fault line between limestone and alluvial deposits. Furthermore, several bedrock collapse sinkholes (BCS) are seen in the limestone south of the lake. The orientations and alignments of the long axes of these dolines are pointed towards the region where recent CCS has developed. This may suggest the existence of an ancient bedrock collapse structure beneath the alluvium. During intense rainfall, the former lake region experiences transient flooding, with surface water draining southward, converging at the fault line and concealed BCS beneath the alluvium. This flow has induced CCS formation due to the concentration of groundwater flow within the intersection zone. The results of this study emphasise that it is necessary to develop integrated hazard mitigation plans, considering hydrology, lithology, structural geology, remote sensing, and geomorphology to address issues such as the KCB and other global problems.

Keywords Sinkhole · Wetland · Remote sensing · Subsidence

Introduction

The increasing global population and changing environmental conditions are causing the swift deterioration of essential natural ecosystems, such as forests, marshes, and lakes, while also intensifying the occurrence and severity of both natural and human-induced disasters (Foley et al. 2005; Hansen et al. 2013; Davidson 2014; IPCC 2023). Wetlands and lakes are distinguished by their high biodiversity level and are among our planet's most valuable ecosystems (Mitsch and Gosselink 2000). They provide various direct and indirect benefits both locally and globally. However, the shifting climatic conditions and the growing human population strain the world's lakes and wetlands (Pekel et al. 2016; Yao et al. 2023). In the last 150 years, more than fifty percent of the world's wetlands have been damaged or destroyed (Davidson 2014), especially in arid and semi-arid regions (Micklin 2016; Demir and Keskin 2020; Vey et al. 2021; Tudryn et al. 2021; Orhan et al. 2024; Akbas 2024). The complete drying up, reduction in size and seasonal variations of these areas lead to many environmental changes (Kuzucuoglu et al. 1998; Scheidt et al. 2005; Gutiérrez 2016; Jiang et al. 2023). The transformation of former lake regions into semi-arid regions for agricultural, residential, or economic purposes has increased groundwater extraction. Groundwater overdraft leads to multiple adverse impacts, including permanent groundwater storage loss, a decline in the groundwater table, land subsidence, and sinkhole formation (Khorrami et al. 2021; Sevil and Gutiérrez 2023; Hasan et al. 2023; Orhan et al. 2024). Subsidence and sinkhole formation are serious geohazards that can significantly impact

✉ Muhammed Zeynel Öztürk
muhammed.zeynel@gmail.com

[1] Department of Geography, Faculty of Humanity and Social Sciences, Niğde Ömer Halisdemir University, Niğde, Türkiye

[2] Department of Geography, Faculty of Arts and Sciences, Ahi Evran University, Kırşehir, Türkiye

[3] Department of Geomatics Engineering, Faculty of Engineering, Sivas Cumhuriyet University, 58140 Sivas, Türkiye

infrastructure and human settlements (Gutiérrez et al. 2014; Brahmi et al. 2023; Eren et al. 2024). Due to these impacts, it is imperative to meticulously observe subsidence, sinkhole development, and alterations in land cover in regions of intensive groundwater utilisation (Minderhoud et al. 2017).

The term 'land subsidence' denotes the vertical descent of the Earth's surface caused by the compaction of aquifer materials due to a decrease in pore pressure (Galloway and Burbey 2011). Subsidence is a widespread global concern with significant and detrimental consequences (Herrera-García et al. 2021; Bagheri-Gavkosh et al. 2021; Hasan et al. 2023). This phenomenon can be ascribed to numerous natural and human-induced factors. The most significant factor is reduced groundwater levels due to excessive extraction (Galloway and Burbey 2011; Khorrami et al. 2021). This tendency is particularly pronounced in arid and semi-arid urban and agricultural regions, such as the KCB (Herrera-García et al. 2021; Bagheri-Gavkosh et al. 2021; Hasan et al. 2023). In such areas, the necessity for irrigation leads to an increased demand for groundwater.

The term 'sinkhole' or 'doline' refers to a closed depression typically linked to the dissolution of carbonate and evaporite rocks. The formation of sinkholes can be attributed to a range of natural and anthropogenic factors, with subsidence representing one of the most significant contributing factors (Gutiérrez et al. 2014). Scientist categorises sinkholes into specific classifications based on their developmental attributes (Waltham and Fookes 2003). In the Anatolian region, collapse sinkholes are called 'obruks', with the KCB as the most active zone for obruk formation. Researchers have identified two distinct groups of obruks in Central Anatolia. Large "old" or "paleo" obruks, situated on the Obruk Plateau and categorised as caprock and bedrock collapse sinkholes (BCS), attain widths up to 900 m (Fig. 1a–d) (Eren et al. 2024). Natural processes caused the formation of the old obruks (Erinç 1960; Eroskay and Günay 1979; Canik and Çörekçioğlu 1986; Erol 1991; Bayarı et al. 2024). The "young" obruks, categorised as cover collapse sinkholes (CCS), have emerged in recent decades and are often measured less than 50 m in diameter (Fig. 1e–f). The emergence of CCS in the KCB is linked to human-induced groundwater extraction (Fig. 1a–d). An unpublished inventory by the General Directorate of State Hydraulic Works of Türkiye (DSİ) indicates that there are over 130,000 groundwater extraction wells in the KCB, with around 80% being unregistered (Şïrecï et al. 2021). The extraction of groundwater in the KCB has resulted in declining groundwater levels. This decline has consequently led to the formation of subsidence and CCS throughout the basin (Doğan and Yılmaz 2011; Ozdemir 2015; Caló et al. 2017; Orhan et al. 2024; Eren et al. 2024). In 2021, researchers identified almost 700 CCS with depths greater than 1 m and 1,850 subsidence and sagging structures, varying from a few meters to 60 m in diameter and with depths of less than 1 m. Most of these are clustered near Karapınar district (Doğan and Yılmaz 2011; Dursun 2022; Arık 2023; Eren et al. 2024; Coşkuner et al. 2025). Nonetheless, the reduction in groundwater levels throughout the basin has resulted in sinkholes in regions where such occurrences had not been previously documented, as demonstrated by the sinkhole formations in the Akgöl Wetland (AW). Since 2010, the desiccation of the AW, a significant wetland in Türkiye, has resulted

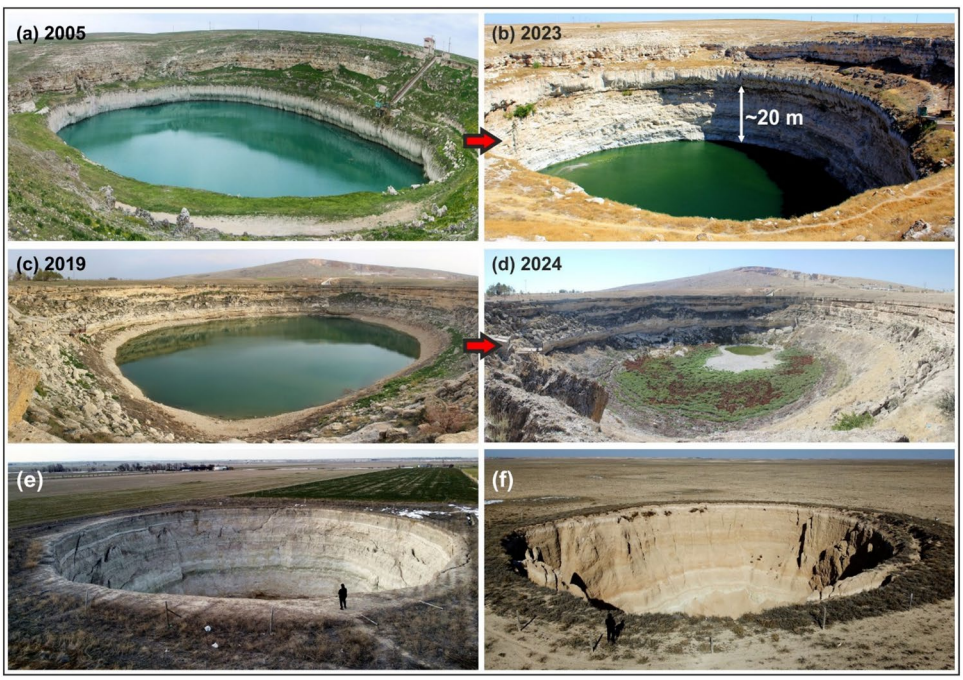

Fig. 1 Change in water levels of the old obruks; **a, b** Kızören Obruk and **c, d** Timraş Obruk. **e, f** Examples of young obruks in the Karapinar region

in subsidence and sinkholes along the former shores of the lake (Fig. 2e–g) (Eren et al. 2021, 2024). The formation of sinkholes presents a significant financial risk, particularly concerning infrastructure damage, and may also result in human casualties. Therefore, monitoring and assessing areas susceptible to sinkhole formation is essential. This study applies a satellite-based methodology, Interferometric Synthetic Aperture Radar (InSAR), Google Earth Engine (GEE), and Corine Land Cover (CLC) to investigate the relationship between subsidence distribution and sinkhole formation in the AW. The underlying causes of high subsidence and sinkhole formation in a dried wetland were elucidated by combining these techniques with field observations.

Study area

The study area is located in the eastern part of the KCB, the largest endorheic basin in Türkiye. The elevation in the KCB varies from 850 to 1,000 m above sea level across the relatively flat plains, with the highest point reaching 3,900 m in the Taurus Mountains (Fig. 2a). The Taurus Mountains, especially the Bolkar Mountains, form the southern and southwestern boundaries of the KCB, acting as the basin's primary water supply. Precipitation and snowmelt from these mountains replenish the ephemeral rivers and groundwater of the basin.

During the last glacial period of the Quaternary, the KCB was submerged beneath a lake called Konya Paleolake, which reached a depth of 20 m (Roberts 1983; Fontugne et al. 1999). Despite the absence of surface outflows, the basin features several karstic outlets to the deeper strata, particularly in the southern section. The principal groundwater

Fig. 2 **a, b** Location and elevation map of KCB and study area; **c** an aerial view of the former lake bed of Akgöl; **d** wind deflation over the former lakebed; **e** an obruk formed in 2019 (Akkaya et al. 2019) and **f** a ponor formed in 2019 in AW (Güngör 2019)

drainage system in the KCB is the flow of groundwater through underground channels directed towards Salt Lake in the north and the Mediterranean Sea in the south (Nazik et al. 2019). These properties likely prevented the complete salinisation of the basin during the paleo-history (Roberts 1983). After the last glacial maximum, rising temperatures resulted in the desiccation of the Konya Paleolake, facilitating the emergence of several wetlands and swamps in the KCB. One of these wetlands is AW, located at 1000 m, which was one of the most extensive wetlands in Türkiye in the 1950s in terms of area (Fig. 2b). It is considered one of the most important avian habitats and one of the largest wetlands in Türkiye, playing a crucial role in a primary migratory route for birds. In 1992, AW was classified as a Class 1 Natural Protection Area; in 1995, it was further designated a Nature Reserve Area. Nevertheless, the wetland has substantially decreased surface area due to human-induced environmental alterations. The drying process of the AW began in the 1950s due to malaria control efforts and subsequent agricultural advancements. The construction of the Ayrancı, İvriz, and Gödet dams in 1958, 1984, and 1988, respectively, within the lake basin has significantly contributed to the desiccation of the lake (Dervişoğlu et al. 2017; Tanık et al. 2018). The current environment features a variety of habitats, including reedbeds, swamps, mud islets, meadows, arid plains, and steppes (Fig. 2c, d).

The Ereğli Meteorological Station, situated 30 km east of the study area, has an average annual temperature of 11.7 °C. The monthly average temperatures decrease to 0 °C during winter and rise to 23.3 °C during summer. The total annual precipitation in the study area, one of the least rainy regions of Türkiye, is 302 mm. The annual evaporation rate is 1.355 mm, leading to a considerable annual water deficit. The average precipitation in August is 4.6 mm in the area characterised by significant summer drought. The climatic data suggest that the study area has a semi-arid climate characteristic (Öztürk et al. 2017; Aydın et al. 2019; Taşoğlu et al. 2024). Despite the arid conditions of the plain, surface runoff from the surrounding mountainous, particularly from the Bolkar Mountains, aids in replenishing the plain (Kuzucuoğlu 2019).

The study area's lithology primarily consists of Quaternary units, with volcanic and volcano-sedimentary formations in the north and metamorphic units in the south. Located south of AW, the metamorphic Meydan Formation (JKme), part of the Bolkar Mountain range (Fig. 3), comprises Jurassic-Cretaceous-aged meta-carbonates. This unit, composed of recrystallised limestones and dolomites, is devoid of fossils (Bilgiç 2009; Ulu 2009). Thirteen BCS exist within these limestones, varying in length from 270 to 710 m, with their long axes aligned in an NW–SE orientation (Fig. 3b).

The Late Pleistocene-Holocene-aged Hotamış Formation (Qho) is the predominant lithologic unit in AW and its surroundings (Fig. 3). It comprises gravels, gravelly sands, silts, and clays. It is subdivided into five members: Börücekyayla, Küpbasan, İsmil, Sazlıpınar, and Bataklık. These members represent depositional sequences from the Konya Paleolake's shoreline to its central basin.

The Börücekyayla Member (Qhob) consists of pebbly sand layers with an approximate thickness of 10 m, while the Küpbasan Member (Qhok) comprises lacustrine shore deposits, reaching around 20 m. The İsmil Member (Qhoi) contains clastic lake bottom sediments, including gravel, sand, clay, silt, and gypsum. In contrast, the Sazlıpınar Member (Qhos) comprises carbonate-rich lacustrine deposits with gypsum nodules and cross-laminated gypsum sands. The Bataklık (Swamp) Member (Qhoba) is distinguished by water-saturated, dark-coloured soils formed due to persistent saturation in swampy depositional settings, accumulating

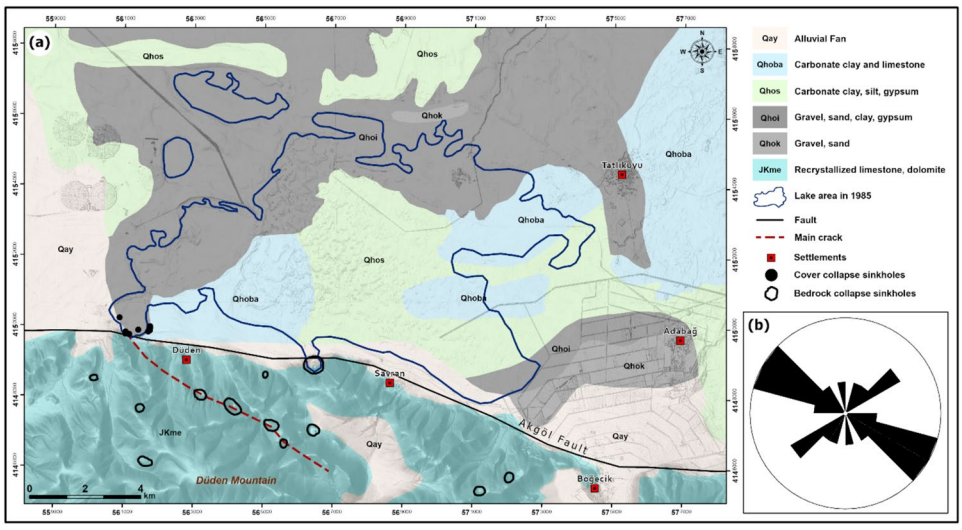

Fig. 3 **a** Lithology map of the study area (Bilgiç 2009; Ulu 2009) and **b** rose diagram of the long axes of bedrock collapse dolines

stained organic-rich soils. The Alluvial Fan (Qay), located south of the study area, also consists of gravelly and sandy limestone and clayey and silty units (Ulu 2009).

Data and method

This study employs a multi-faceted approach, utilising *Interferometric Synthetic Aperture Radar* (InSAR), *Google Earth Engine* (GEE), and *Corine Land Cover* (CLC) change features to analyse the dynamics of AW and its surroundings, with a particular focus on temporal and spatial changes (Table 1). The following sections describe these methods in detail, highlighting their contributions to the study.

Google Earth Engine (GEE)

GEE, a powerful platform, enables efficient observation and processing of multi-sensor satellite imagery without local storage, rapidly handling large datasets and multiple images within a single workflow (Gorelick et al. 2017). The GEE has become the preferred tool in numerous studies, particularly those involving time series analysis, such as the exploration of changes in land cover (Pekel et al. 2016; Chen et al. 2017; Gürbüz 2023). This study used GEE to analyse long-term (1985–2023) areal and temporal changes in the AW, processing over 400 Landsat (TM, ETM+, OLI) images available on the platform.

In the initial stages of data processing, a comprehensive study area boundary was delineated to encompass the entire region surrounding the lake. Filtering out cloud cover was applied when retrieving images from the relevant Landsat libraries. Water surface extraction was performed using images from Landsat 5 satellite between 1985 and 2011. ETM images were avoided as much as possible due to the failure in the scan line corrector mechanism of the Landsat 7 satellite in 2003. The images of this satellite were only used to represent the lake area in 2012–2013. Missing linear areas in the analysis were corrected as polygons after a manual correction process. Landsat 8 images were used for lake area representation between 2014 and 2023.

The NDWI is one of the most critical remote sensing indexes, and it is frequently employed to differentiate water bodies within land cover classifications. Many researchers have conducted comprehensive studies on mapping water bodies, including lakes and monitoring them based on NDWI or its modified forms (McFeeters 1996; Ashok et al. 2021; Ismail et al. 2022; Sha et al. 2022; Li et al. 2022; Atesoglu et al. 2025).

In this study, images were rapidly acquired using the GEE platform and the NDWI equation was applied. Annual and seasonal (summer and winter) area values were calculated and compared during the NDWI application. Summer was represented by July, August, and September to represent the effect of surface temperature on evaporation, while winter was similarly defined by January, February, and March. The raster-based images obtained within the scope of the prepared study area were saved by creating a geographical database, and the analysis part was completed. The NDWI equation creates result maps that produce values between -1 and 1. The threshold value recommended by (McFeeters 1996) for the extraction of water and land in the index results is 0. Positive values represent water, and negative values represent land areas. However, since the effect of the distinction between water and land on the reflectance values recorded by satellites depends on land cover components such as shadow, forest, built-up, clouds, and snow, setting a fixed number as a threshold value makes it difficult to establish precise boundaries in the extraction of water areas (Ji et al. 2009; Acharya et al. 2018). Since AW is a shallow lake with a low water level, while determining the specific threshold values for each index map in the inference of the water area, the values following the lake boundaries were determined separately for each index map by visual interpretation of the index results. This way, the shallow regions constituting the lake's boundaries were also evaluated. In the post-processing stage, the lake boundaries were extracted as a vector using the uniquely determined threshold values. The lake's areal change was analysed with a 39-year temporal series based on each year's summer and winter seasons. In 39 years, seasonal and annual areas of the lake were calculated and visualised graphically (Fig. 4a). GEE analysis yielded comprehensive insights into the long-term seasonal and yearly fluctuations

Table 1 The spatial resolution and the time interval of the datasets used in the study

Method	Dataset	Resolution	Period	Purpose
InSAR	Sentinel-1 A/B	100 m	2014–2023	Subsidence rates, earth surface deformation
GEE	Landsat 5 TM	30 m	1985–2011	Water surface changes
	Landsat 7 ETM+	30 m	2012–2013	
	Landsat 8 OLI	30 m	2014–2023	
CLC	Landsat, Sentinel	100 m	1990 and 2018	Land cover changes

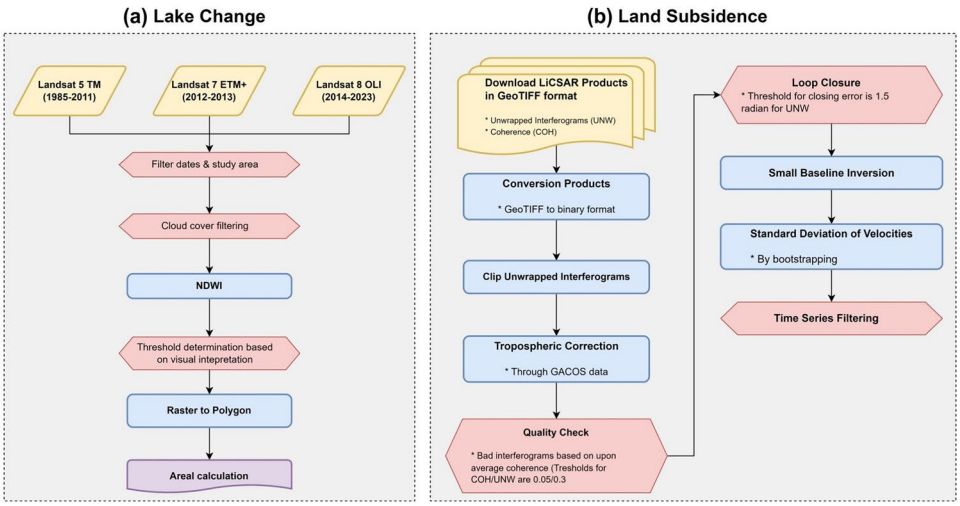

Fig. 4 **a** The water area extraction analysis flow chart. The first part shows the data pre-processing and the NDWI analysis with GEE, while the last part shows the post-processing of the methodology and information extraction. **b** The processing workflow of LiCSBAS open-source software (Morishita et al. 2020)

in the AW's surface area. This analysis provided detailed insights into the AW's surface area's long-term seasonal and annual changes. In addition, the methodology framework of this analysis reveals the ease of GEE in processing big data and its strengths in temporal series analysis.

Corine Land Cover (CLC)

The desiccation of wetlands and lakes leads to significant land cover changes (Caló et al. 2017; Assefa et al. 2021), especially in arid and semi-arid regions, where water loss creates salt pans or playas due to mineral-rich water evaporation (Bilgilioğlu et al. 2021). Additionally, the exposure of dry lakebeds and wetland sediments to aeolian erosion often forms dunes (Kuzucuoglu et al. 1998) (Fig. 2d). These transformations impact both the physical environment and ecosystems, causing habitat loss, reduced biodiversity, and disruptions to ecosystem services (Erwin 2009).

Monitoring land use and cover changes over time is crucial for understanding the interactions between human activities and natural processes. This supports informed decision-making in land management, conservation, and sustainable development. The CLC system, based on satellite imagery interpretation, is widely used in Europe to analyse land use changes, providing national-scale maps every six years for 39 countries (Popovici et al. 2013; Büttner 2014).

This study used CLC maps from 1990 and 2018 to assess AW's land cover changes and surroundings. A 352 km^2 area within a 5 km buffer around the 1985 wetland boundary was analysed, revealing long-term trends such as agricultural expansion, urbanisation, and habitat loss.

Interferometric Synthetic Aperture Radar (InSAR)

In addition to GEE, this study employed InSAR to assess surface deformation, revealing land subsidence in the former lake area and its surroundings over the past nine years following desiccation.

InSAR, a technique that detects surface deformations by comparing radar images from different orbital passes, has proven reliable for monitoring subsidence and groundwater storage depletion (Higgins et al. 2014). This method requires analysing many interferograms, an inherently time-consuming process. The Centre for the Observation and Modelling of Earthquakes, Volcanoes, and Tectonics (COMET 2024) provides freely downloadable Sentinel-1A/B interferograms, operated by the European Space Agency (ESA), coherence data and unwrapped/ geocoded interferograms with 0.001° spatial resolution using the Looking into Continents from Space with Synthetic Aperture Radar (LiCSAR) system (Morishita et al. 2020; COMET 2024).

To conduct a comprehensive examination of subsidence in the AW, LiCSAR products were employed for both ascending track 087 (frame 05317) and descending track 167 (frame 05276), encompassing the period from October 2014 to May 2023 (Morishita et al. 2020). A total of 1,521 interferograms and coherence data for ascending orbits and 1,291 for descending orbits were processed using a small baseline interferogram inversion approach through the LiCSBAS open-source software (Morishita et al. 2020, 2023; Morishita 2021). The LiCSBAS is an open-source software package for analysing InSAR time series that can be used with LiCSAR products. The LiCSBAS software was selected for its compatibility with the LiCSAR products, offering significant advantages in terms of time efficiency and disk space optimisation during interferogram generation, as well as its effectiveness in processing large interferogram datasets. Figure 4b demonstrates the general processing workflow.

The Generic Atmospheric Correction Online Service data were applied to ascending and descending frames to reduce tropospheric noise (Yu et al. 2018). Furthermore, unwrapping errors exceeding 1.5 radians RMS of the loop phase

for the closure of three interferograms were discarded from the processing. Next, we utilised the small baseline network inversion to calculate the deformation time series (López-Quiroz et al. 2009). A temporal interpolation technique was employed to address gaps within the interferogram network, assuming a linear deformation trend over the long term. Subsequently, a low-pass filter was applied manner spatially.

The Low-pass filtering spatially employs attenuation of high-frequency components, often associated with noise, within spatial data. This method achieves spatial smoothing of deformations by diffusively averaging values across adjacent data points, thereby reducing abrupt variations and enhancing the continuity of small-scale fluctuations. In addition, a high-pass filter was used manner temporally. The high-pass temporal filter is utilised to preserve high-frequency variations, such as rapid changes, while attenuating low-frequency components, including long-term trends and periodic oscillations like annual cycles. Both were employed to enhance the signal-to-noise ratio and emphasise long-term deformations.

Results

The GEE analyses indicate that AW's surface area displays significant seasonal fluctuation. The water surface area of AW, roughly 53 km^2 during the winter of 1985, significantly decreased to 0.54 km^2 by the winter of 2023. In the summer of 1985, the water body was estimated to have an area of around 29 km^2. By the summer of 2023, the surface area had decreased to 0.41 km^2 (Fig. 5a), marking a nearly 99% reduction in AW's water area. The decrease in the area of the lake prompted the construction of a filling embankment approximately 7 km in length and 1.5 m in height in the northern part of the lake in 2014 (Fig. 7a). As part of the reclamation works, water was transported through water canals. The implementation has resulted in the formation of a small, permanent water body during summer (Fig. 5b).

The submerged portion of the lake is now small, and increasing human activity in and around the former lake region has significantly altered the land cover. The lake's disappearance has led to marshes and salt marshes. A 5 km buffer zone established in 1985 (Fig. 6) shows that salt marshes emerged on the lakebed between 1990 and 2018, expanding to 665 ha. Their formation coincided with surface runoff, particularly in the southwest, where sinkholes are present. Marshland has also expanded, and pastureland has grown, especially in the east, replacing natural grasslands. Due to nearby small villages, artificial area expansion has remained limited (Fig. 6).

Subsidence rates from October 2014 to May 2023 highlight significant ground deformation in the study area. InSAR results indicate annual subsidence of 15–33 mm in the southern part of the AW (Fig. 7a–b). This region, the lowest elevation zone, consists of Quaternary units overlying limestones, where high subsidence aligns with the Akgöl Fault line separating the geological units (Eren et al. 2025). The CCS is located near the Akgöl Fault, covered by lake sediments, which play a crucial role in subsidence and sinkhole formation by creating zones of weakness that facilitate fluid movement. The alignment of high subsidence in the study area follows the fault lines, while the intersection of the fault with surface water runoff from rainwater influences CCS development.

To analyse the temporal characteristics of subsidence, time series were generated from two locations (Site 1 and Site 2) exhibiting elevated subsidence rates. The time series for Site 2 indicates that the total sinking during nine years amounted to 232 mm. A seasonal subsidence pattern is seen in the study area, with the most pronounced seasonality observed at Site 1 (Fig. 7c). Additionally, a significant increase in subsidence levels has been recorded at Site 2 since 2019 (Fig. 7d). The InSAR time series data indicate that subsidence rates escalate during intervals of reduced precipitation, attributed to a decrease in the water table.

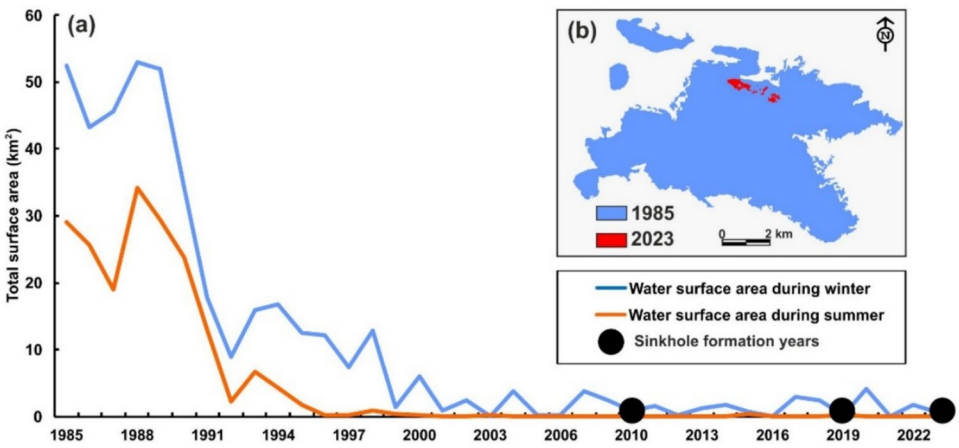

Fig. 5 **a** Variations in lake surface area throughout winter and summer from 1985 to 2023, accompanied by sinkhole formation. **b** The AW's surface area in 1985 and 2023

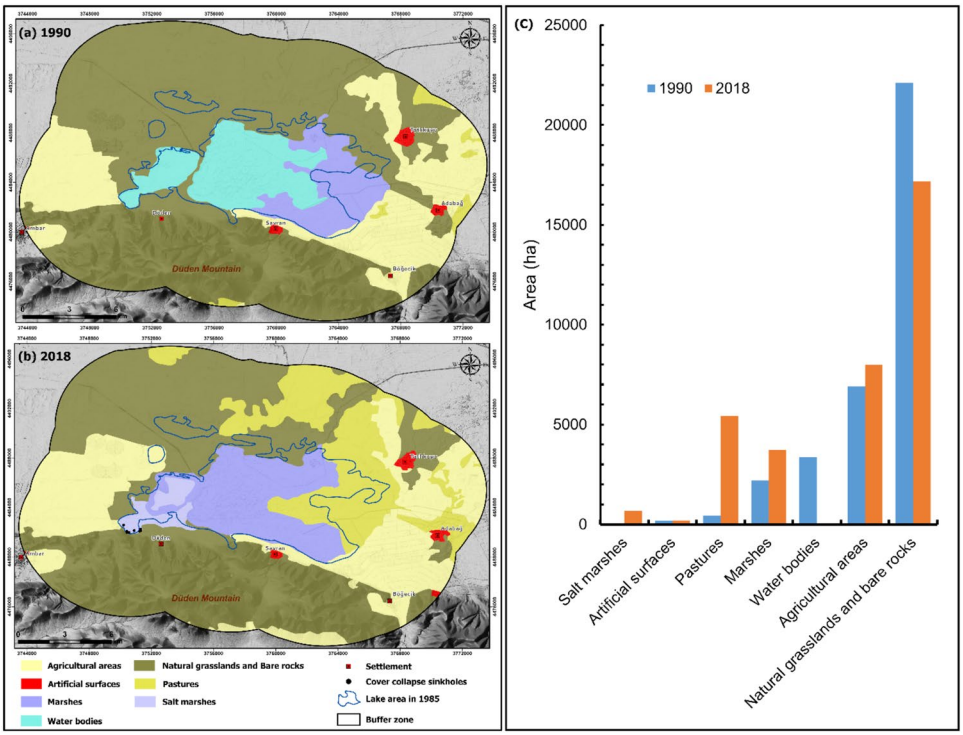

Fig. 6 Spatial distribution of land cover for **a** 1990 and **b** 2018. **c** The changes in land cover between two periods

Discussion

The KCB is the largest closed basin in Türkiye, encompassing numerous lakes and wetlands, but faces severe water-related issues. Climate change and inefficient water management policies have exacerbated these issues, especially in the agricultural sector (Caló et al. 2017). The surface waters and groundwater in the KCB are extensively utilised for agricultural purposes. The construction of dams in the KCB, characterised by a semi-arid climate, has reduced surface water flow and led to decreased groundwater levels due to the installation of water wells (Yılmaz et al. 2021). Water well data reveals a significant acceleration in groundwater level decline in the KCB, particularly since 2014 (Fig. 1c–d), with water levels dropping by approximately 3–4 m annually (Üstün et al. 2015; Orhan 2021; Şïrecï et al. 2021). This situation has resulted in the formation of cover collapse sinkholes and the occurrence of varying rates of subsidence in the KCB (Bayari et al. 2009; Üstün et al. 2010, 2015; Doğan and Yılmaz 2011). The Karapinar region is undergoing land subsidence and sinkhole development due to significant groundwater extraction that began in the early 2000s (Orhan et al. 2024). Over-extraction of groundwater in agricultural regions has led to a decline in the water table by ~ 4 m per year from 2014 to 2019, causing subsidence of 8 cm per year in the Konya metropolitan area (Şïrecï et al. 2021). Groundwater levels decreased by 20–24 m from 2000 to 2022 (Orhan et al. 2024). In addition to accelerating subsidence, seasonal variations in subsidence are also noticed. This seasonal pattern of subsidence follows the temporal fluctuations in groundwater levels (Üstün et al. 2015; Gezgin 2022; Orhan et al. 2024).

In recent years, the occurrence of land subsidence and the formation of sinkholes in the KCB has been identified and monitored using InSAR observations (Üstün et al. 2010, 2015; Caló et al. 2017; Orhan et al. 2024). One of the most notable findings is the increase in the subsidence rate over time. For example, in Konya City, the subsidence rate rose from 15 mm/year between 1995 and 2000 to 30 mm/year between 2002 and 2010 and to 50 mm/year from 2014 to 2015 (Üstün et al. 2015; Canaslan Comut 2016). A further study found that the subsidence rate increased from a few cm per year to 11 cm per year between 2014 and 2019 (Şïrecï et al. 2021). Our study recorded the highest total subsidence, 232 mm, over the observation periods (Table 2).

The formation of sinkholes in the KCB is primarily linked to the distribution of faults, subsidence, and groundwater extraction (Doğan and Yılmaz 2011; Coşkuner et al. 2021; Eren et al. 2021, 2024, 2025; Bayarı et al. 2024; Orhan et al. 2024). The density and extent of cracks and faults significantly influence subsidence and sinkhole development by creating zones of weakness that facilitate fluid movement (Burbey 2002; Cigna et al. 2011; Hu et al. 2019; Eren et al. 2021; Vassileva et al. 2021; Raspini et al. 2022). The regions most affected by subsidence and sinkhole formation in the KCB coincide with fault distributions, often lying by Quaternary sediments (Şïrecï et al. 2021; Arık 2023; Orhan et al. 2024; Eren et al. 2024). This study highlights a connection

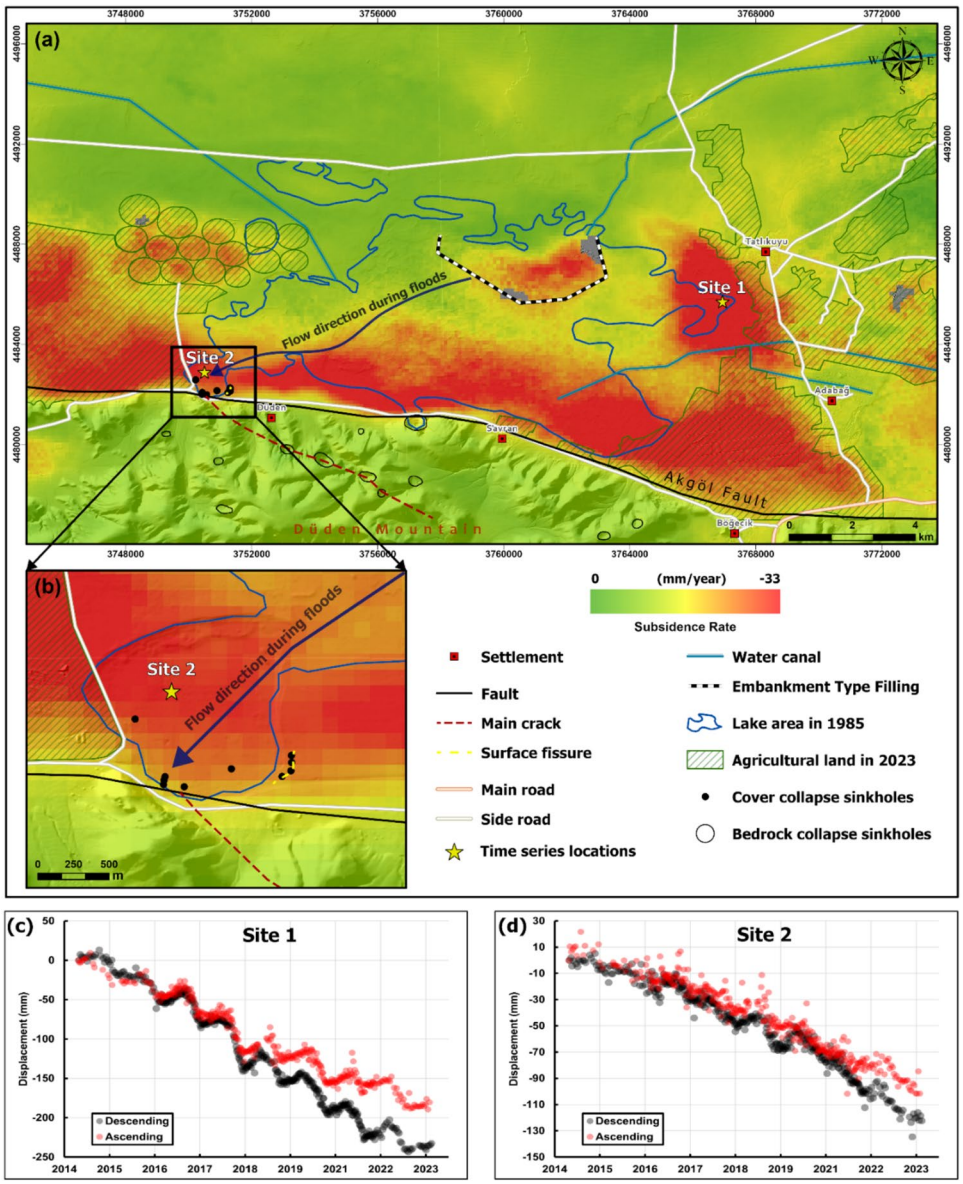

Fig. 7 **a, b** InSAR deformation maps show the vertical component derived from ascending and descending orbits using LICSAR products. **c, d** InSAR time series data at Site 1 and Site 2 for ascending and descending orbits

Table 2 Subsidence values determined by InSAR method in KCB

References	Study area	Period	Annual subsidence rate	Maximum rate (Local rate)	Total subsidence
(Üstün et al. 2010)	KCB	2006–2009	12–52 mm/year		
(Üstün et al. 2015)	KCB	2002–2009	10–40 mm/year		
(Canaslan Comut 2016)	Konya city	1995–2015	30–60 mm/year	50 mm/year	
(Caló et al. 2017)	Eastern part of KCB	2002–2010	12 mm/year		100 mm
(Ahmed et al. 2020)	KCB	2011–2014	50 mm/year		200 mm
(Weiss et al. 2020)	KCB	2014–2019	> 50 mm/year		
(Orhan 2021)	Konya city	2014–2018		75 mm/year	200 mm
(Şirecï et al. 2021)	Konya city	2014–2019	60–70 mm/year	110 mm/year	
(Yeşilmaden et al. 2021)	KCB	2016–2019	17 mm/year		160 mm
(Gezgin 2022)	Karaman province	2016–2021	25 mm/ year in city centre	50 mm/year	
(Orhan et al. 2024)	Karapınar Region	2014–2018	25 mm/year	70 mm/year	100 mm
This study	Akgöl Wetland	2014–2023	15–30 mm/year	50 mm/year	232 mm

between seasonal surface runoff in dried lake areas and sinkhole occurrence, particularly where it intersects with the Akgöl Fault, main crack and high subsidence zones.

The Akgöl Fault is intersected by NW–SE and NE-SW oriented transfer faults, subsidence-related surface fissures, and surface faulting (Eren et al. 2025). Figures 3 and 7a reveal thirteen BCS in the limestone south of AW, aligned NW–SE toward the CCS formation area. The orientation of BCS generally matches fault and crack lines (Öztürk et al. 2018a, b), suggesting two potential mechanisms for their role in covered collapse sinkhole formation in AW. The first hypothesis posits that subsidence dolines, buried under alluvium, lie beneath the current sinkholes and align with BCS extensions. The second proposes a significant NW–SE trending crack system alongside the Akgöl Fault. Given the interrelationship between subsidence, sinkholes, BCS, seasonal runoff, and faults, it is imperative to conduct precise fault mapping and monitor temporal changes in lake surfaces in regions where subsidence and sinkholes pose a risk, as well as to undertake a comprehensive investigation into the interactions among these phenomena.

Conclusion

The AW has undergone significant subsidence in recent years, accompanied by the formation of numerous sinkholes. The annual average subsidence rate in the former lake area ranges from 15 mm/year to 30 mm/year, resulting in a total subsidence of 232 mm between 2014 and 2023. The highest subsidence rates are concentrated in the southern part of the former lake, particularly along the limestone, where structural weaknesses and fault activity play a crucial role. Recent CCS formations in this region are primarily attributed to the intersection of the surface runoff direction with fault lines, particularly along the Akgöl Fault and associated crack lines.

In addition to the region's tectonics, the BCS in the south of the area is oriented to the current sinkhole area. These tectonic and geomorphologic highlights are two possible mechanisms driving sinkhole formation in the AW. First, BCS buried beneath alluvium may exist beneath the current sinkholes. Second, a significant crack system, extending in NW–SE direction in addition to the Akgöl Fault, likely enhances subsidence processes. These structural weaknesses, surface water infiltration and seasonal fluctuations in groundwater levels contribute to progressive land deformation.

Time-series analyses indicate that while subsidence exhibits seasonal variability, its rate has accelerated markedly in recent years. This trend suggests an increasing risk of further sinkhole formation, particularly in areas that have already experienced substantial ground deformation. Given the interrelationship between subsidence, sinkholes, collapse dolines, seasonal runoff, and fault activity, conducting high-precision fault mapping and monitoring temporal changes in lake surfaces is critical. Furthermore, a comprehensive investigation into the interactions among these processes is necessary to assess future risks and develop mitigation strategies for the affected areas.

Acknowledgements We want to thank the reviewers for their valuable contributions to the study. Besides, Muhammed Zeynel Öztürk thanks the Turkish Academy of Sciences for their support within the Outstanding Young Scientist Award Program (TÜBA-GEBIP-2023).

Author contributions Muhammed Zeynel Öztürk: Conceptualization, Data curation, Formal Analysis, Methodology, Resources, Supervision. Visualisation, Writing—Original Draft, Writing – Review and Editing Murap Poyraz: Data curation, Formal Analysis, Visualization, Investigation, Writing—Review & Editing Hüseyin Duman: Data curation, Formal Analysis, Visualization, Writing—Review & Editing Enes Taşoğlu: Data curation, Formal Analysis, Visualization, Writing—Review & Editing.

Funding Open access funding provided by the Scientific and Technological Research Council of Türkiye (TÜBİTAK). There was no funding obtained for this study.

Data availability No datasets were generated or analysed during the current study.

Declarations

Conflict of interest The authors declare no competing interests.

References

Acharya TD, Subedi A, Lee DH (2018) Evaluation of water indices for surface water extraction in a landsat 8 scene of Nepal. Sensors (Switzerland) 18:1–15. https://doi.org/10.3390/s18082580

Ahmed AW, Kalkan E, Guzy A et al (2020) Modeling of land subsidence caused by groundwater withdrawal in Konya Closed Basin, Turkey. Proc IAHS 382:397–401. https://doi.org/10.5194/piahs-382-397-2020

Akbas A (2024) Human or climate? Differentiating the anthropogenic and climatic drivers of lake storage changes on spatial perspective via remote sensing data. Sci Total Environ 912:168982. https://doi.org/10.1016/j.scitotenv.2023.168982

Akkaya İ, Dönmez H, Atmaca, A. A (2019) Akgöl'ün kenarında obruklar oluştu. Doğan Haber Ajansı

Arık F (2023) Dünya'da ve Türkiye'de obruk oluşumları: tanım, sınıflandırma ve oluşum koşulları. In: Kavak O, Haspolat YK (eds) Farklı Yaklaşımlarla Mineraller ve Doğal Taşlar. Orient Yayınları, pp. 121–155

Ashok A, Rani HP, Jayakumar KV (2021) Monitoring of dynamic wetland changes using NDVI and NDWI based landsat imagery. Remote Sens Appl: Soc Environ 23:100547. https://doi.org/10.1016/j.rsase.2021.100547

Assefa WW, Eneyew BG, Wondie A (2021) The impacts of land-use and land-cover change on wetland ecosystem service values in peri-urban and urban area of Bahir Dar City, Upper Blue Nile Basin. Northwestern Ethiopia Ecol Process 10:39. https://doi.org/10.1186/s13717-021-00310-8

Atesoglu A, Ozel HB, Varol T et al (2025) Monitoring Land Cover/Use Conversions in Türkiye Wetlands Using Collect Earth. J Indian Soc Remote Sens. https://doi.org/10.1007/s12524-024-02111-w

Aydın S, Şimşek M, Çetinkaya G, Öztürk MZ (2019) Regime Characteristics of Turkey's Climatic Regions Determined Using the Erinç Precipitation Efficiency Index. In: 1st Istanbul International Geography Congress Proceedings Book. İstanbul, pp 752–760

Bagheri-Gavkosh M, Hosseini SM, Ataie-Ashtiani B et al (2021) Land subsidence: A global challenge. Sci Total Environ 778:146193. https://doi.org/10.1016/j.scitotenv.2021.146193

Bayari CS, Pekkan E, Ozyurt NN (2009) Obruks, as giant collapse dolines caused by hypogenic karstification in central Anatolia, Turkey: Analysis of likely formation processes. Hydrogeol J 17:327–345. https://doi.org/10.1007/s10040-008-0351-9

Bayarı S, Özyurt Y, Nazik L et al (2024) Role of hypogenesis in the evolution of karst in the Taurus Mountains Range, Turkey. Int J Speleol 53:11–128

Bilgiç T (2009) 1/100.000 scale Turkish Geology Maps, Karaman N31 sheet.

Bilgilioğlu BB, Erten E, Musaoğlu N (2021) Analysis of salt lake volume dynamics using sentinel-1 based SBAS measurements: a case study of Lake Tuz. Turkey Remote Sens 13:2701. https://doi.org/10.3390/rs13142701

Brahmi S, Fehdi C, Hadji R et al (2023) Karst-induced sinkhole detection using a tomography imaging survey, case of setifian high plain, NE Algeria. Geotech Geol Eng 41:1961–1976. https://doi.org/10.1007/s10706-023-02384-x

Burbey T (2002) The influence of faults in basin-fill deposits on land subsidence, Las Vegas Valley, Nevada, USA. Hydrogeol J 10:525–538. https://doi.org/10.1007/s10040-002-0215-7

Büttner G (2014) CORINE Land Cover and Land Cover Change Products. In: Manakos I, Braun M (eds) Land Use and Land Cover Mapping in Europe. Springer, Netherlands, Dordrecht, pp 55–74

Caló F, Notti D, Galve J et al (2017) DInSAR-based detection of land subsidence and correlation with groundwater depletion in Konya Plain. Turkey Remote Sens 9:83. https://doi.org/10.3390/rs9010083

Canaslan Comut F (2016) Detecting of surface deformations on different ground characteristics using advanced InSAR techniques. Doctoral dissertation, School of Natural and Applıed Scıence, Selcuk University, (in Turkish)

Canik B, Çörekçioğlu İ (1986) The Formation of Sinkholes (Obruk) Between Karapınar and Kızören-Konya. IAHS AISH Publ 161:193–205

Chen B, Xiao X, Li X et al (2017) A mangrove forest map of China in 2015: Analysis of time series Landsat 7/8 and Sentinel-1A imagery in Google Earth Engine cloud computing platform. ISPRS J Photogramm Remote Sens 131:104–120. https://doi.org/10.1016/j.isprsjprs.2017.07.011

Cigna F, Cabral-Cano E, Osmanoglu B et al (2011) Detecting subsidence-induced faulting in Mexican urban areas by means of Persistent Scatterer Interferometry and subsidence horizontal gradient mapping. 2011 IEEE International Geoscience and Remote Sensing Symposium. IEEE, Vancouver, BC, Canada, pp 2125–2128

COMET (2024) COMET-LiCS Sentinel-1 InSAR portal. In: https://comet.nerc.ac.uk/COMET-LiCS-portal/

Coşkuner B, İnce İ, Barstuğan M (2025) Sinkhole detection via deep learning using DEM images. Nat Hazards. https://doi.org/10.1007/s11069-025-07127-0

Coşkuner B, Eren Y, Parlar Ş (2021) Karapınar (Konya, Orta Anadolu) bölgesindeki obruklar, kırıklar ve otomatik belirlenmiş çizgisellikler arasindaki ilişki

Davidson NC (2014) How much wetland has the world lost? Long-term and recent trends in global wetland area. Mar Freshwater Res 65:934. https://doi.org/10.1071/MF14173

Demir V, Keskin AÜ (2020) Water level change of lakes and sinkholes in Central Turkey under anthropogenic effects. Theor Appl Climatol 142:929–943. https://doi.org/10.1007/s00704-020-03347-5

Dervişoğlu A, Musaoğlu N, Tanık A et al (2017) Satellite-Based Temporal assessment of a dried lake: Case study of Akgol Wetland. Fresenius Environ Bull 26:352–359

Doğan U, Yılmaz M (2011) Natural and induced sinkholes of the Obruk Plateau and Karapınar-Hotamış Plain, Turkey. J Asian Earth Sci 40:496–508. https://doi.org/10.1016/j.jseaes.2010.09.014

Dursun AE (2022) Risk analysis of natural sinkholes hazards in Karapınar basin (Konya, Turkey). Arab J Geosci 15:279. https://doi.org/10.1007/s12517-022-09564-8

Eren Y, Parlar Ş, Coşkuner B, Arslan Ş (2024) Geological and Morphological Features of the Karapınar Sinkholes (Konya, Central Anatolia, Türkiye). J Earth Sci 35:1654–1668. https://doi.org/10.1007/s12583-023-1853-z

Eren Y, Coşkuner B, Parlar Ş (2025) An Example of Intracontinental Cross Faults Formation from the Vicinity of Karapınar (Konya – Central Anatolia). Acta Geolog Polon 75:35–35

Eren Y, Parlar Ş, Coşkuner B, Arslan Ş (2021) Sinkhole Formation in Hotamis-Akgöl Basins In The South Of Karapinar (Konya, Central Anatolia). pp 18–19

Erinç S (1960) On the karst features in Turkey. Turkish Geographical Review 20:1–14

Erol O (1991) The Relationship between the Phases of the Development of the Konya-Karapinar Obruks and the Pleistocene Tuz Gölü and Konya Pluvial Lakes, Turkey. J Istanbul Univ Inst Mar Sci Geograph 7:5–49 (**(in Turkish)**)

Eroskay O, Günay G (1979) Tecto-genetic classification and hydrogeological properties of the karst regions in Turkey. In: International Seminar on Karst Hydrogeology. pp 1–41

Erwin KL (2009) Wetlands and global climate change: the role of wetland restoration in a changing world. Wetlands Ecol Manage 17:71–84. https://doi.org/10.1007/s11273-008-9119-1

Foley JA, DeFries R, Asner GP et al (2005) Global consequences of land use. Science 309:570–574. https://doi.org/10.1126/science.1111772

Fontugne M, Kuzucuoğlu C, Karabiyikoğlu M et al (1999) From Pleniglacial to Holocene: a 14C chronostratigraphy of environmental changes in the Konya Plain, Turkey. Quatern Sci Rev 18:573–591. https://doi.org/10.1016/S0277-3791(98)90098-1

Galloway DL, Burbey TJ (2011) Review: Regional land subsidence accompanying groundwater extraction. Hydrogeol J 19:1459–1486. https://doi.org/10.1007/s10040-011-0775-5

Gezgin C (2022) The influence of groundwater levels on land subsidence in Karaman (Turkey) using the PS-InSAR technique. Adv Space Res 70:3568–3581. https://doi.org/10.1016/j.asr.2022.08.003

Gorelick N, Hancher M, Dixon M et al (2017) Google Earth Engine: Planetary-scale geospatial analysis for everyone. Remote Sens Environ 202:18–27. https://doi.org/10.1016/j.rse.2017.06.031

Güngör Y (2019) Akgöl Sazlıkları'nda yeni 2 obruk oluştu. Anadolu Ajansı
Gürbüz E (2023) Monitoring spatio-temporal changes in wetlands with harmonized image series in Google Earth Engine. Environ Monit Assess 195:770. https://doi.org/10.1007/s10661-023-11400-9
Gutiérrez F, Parise M, De Waele J, Jourde H (2014) A review on natural and human-induced geohazards and impacts in karst. Earth Sci Rev 138:61–88. https://doi.org/10.1016/J.EARSCIREV.2014.08.002
Gutiérrez F (2016) Sinkhole Hazards. In: Oxford Research Encyclopedia of Natural Hazard Science. Oxford University Press
Hansen MC, Potapov PV, Moore R et al (2013) High-Resolution Global Maps of 21st-Century Forest Cover Change. Science 342:850–853. https://doi.org/10.1126/science.1244693
Hasan MF, Smith R, Vajedian S et al (2023) Global land subsidence mapping reveals widespread loss of aquifer storage capacity. Nat Commun 14:6180. https://doi.org/10.1038/s41467-023-41933-z
Herrera-García G, Ezquerro P, Tomás R et al (2021) Mapping the global threat of land subsidence. Science 371:34–36. https://doi.org/10.1126/science.abb8549
Higgins SA, Overeem I, Steckler MS et al (2014) InSAR measurements of compaction and subsidence in the Ganges-Brahmaputra Delta, Bangladesh. JGR Earth Surface 119:1768–1781. https://doi.org/10.1002/2014JF003117
Hu L, Dai K, Xing C et al (2019) Land subsidence in Beijing and its relationship with geological faults revealed by Sentinel-1 InSAR observations. Int J Appl Earth Obs Geoinf 82:101886. https://doi.org/10.1016/j.jag.2019.05.019
IPCC (2023) Climate Change 2021 – The Physical Science Basis: Working Group I Contribution to the Sixth Assessment Report of the Intergovernmental Panel on Climate Change, 1st edn. Cambridge University Press
Ismail MA, Waqas M, Ali A et al (2022) Enhanced index for water body delineation and area calculation using Google Earth Engine: a case study of the Manchar Lake. J Water Clim Change 13:557–573. https://doi.org/10.2166/wcc.2021.282
Ji L, Zhang L, Wylie B (2009) Analysis of dynamic thresholds for the normalized difference water index. Photogramm Eng Remote Sens 75:1307–1317
Jiang H, Balz T, Li J, Mishra V (2023) Preliminary investigation of sudden ground subsidence and building tilt in Balitai Town, Tianjin City, on 31 May 2023. Remote Sens 15:4891. https://doi.org/10.3390/rs15194891
Khorrami B, Arik F, Gunduz O (2021) Land deformation and sinkhole occurrence in response to the fluctuations of groundwater storage: an integrated assessment of GRACE gravity measurements, ICESat/ICESat-2 altimetry data, and hydrologic models. Gisci Remote Sens 58:1518–1542. https://doi.org/10.1080/15481603.2021.2000349
Kuzucuoglu C, Parish R, Karabiyikoglu M (1998) The dune systems of the Konya Plain (Turkey): their relation to environmental changes in Central Anatolia during the Late Pleistocene and Holocene. Geomorphology 23:257–271. https://doi.org/10.1016/S0169-555X(98)00008-7
Kuzucuoğlu C (2019) Geomorphological Landscapes in the Konya Plain and Surroundings. In: Çiner A, Kazancı N (eds) Landscapes and Landforms of Turkey. World Geomorphological Landscapes. Springer, Cham, pp 353–368
Li J, Meng Y, Li Y et al (2022) Accurate water extraction using remote sensing imagery based on normalized difference water index and unsupervised deep learning. J Hydrol 612:128202. https://doi.org/10.1016/j.jhydrol.2022.128202
López-Quiroz P, Doin M-P, Tupin F et al (2009) Time series analysis of Mexico City subsidence constrained by radar interferometry. J Appl Geophys 69:1–15. https://doi.org/10.1016/j.jappgeo.2009.02.006
McFeeters SK (1996) The use of the Normalized Difference Water Index (NDWI) in the delineation of open water features. Int J Remote Sens 17:1425–1432. https://doi.org/10.1080/01431169608948714
Micklin P (2016) The future Aral Sea: hope and despair. Environ Earth Sci 75:844. https://doi.org/10.1007/s12665-016-5614-5
Minderhoud PSJ, Erkens G, Pham VH et al (2017) Impacts of 25 years of groundwater extraction on subsidence in the Mekong delta. Vietnam Environ Res Lett 12:064006. https://doi.org/10.1088/1748-9326/aa7146
Mitsch WJ, Gosselink JG (2000) The value of wetlands: importance of scale and landscape setting. Ecol Econ 35:25–33. https://doi.org/10.1016/S0921-8009(00)00165-8
Morishita Y (2021) Nationwide urban ground deformation monitoring in Japan using Sentinel-1 LiCSAR products and LiCSBAS. Prog Earth Planet Sci 8:6. https://doi.org/10.1186/s40645-020-00402-7
Morishita Y, Lazecky M, Wright T et al (2020) LiCSBAS: An Open-Source InSAR Time Series Analysis Package Integrated with the LiCSAR Automated Sentinel-1 InSAR Processor. Remote Sens 12:424. https://doi.org/10.3390/rs12030424
Morishita Y, Sugimoto R, Nakamura R et al (2023) Nationwide urban ground deformation in Japan for 15 years detected by ALOS and Sentinel-1. Prog Earth Planet Sci 10:66. https://doi.org/10.1186/s40645-023-00597-5
Nazik L, Poyraz M, Karabıyıkoğlu M (2019) Karstic Landscapes and Landforms in Turkey. In: Kuzucuoğlu C, Çiner A, Kazancı N (eds) Landscapes and Landforms of Turkey. Springer, Cham, pp 181–196
Orhan O (2021) Monitoring of land subsidence due to excessive groundwater extraction using small baseline subset technique in Konya. Turkey Environ Monit Assess 193:174. https://doi.org/10.1007/s10661-021-08962-x
Orhan O, Haghshenas Haghighi M, Demir V et al (2024) Spatial and Temporal Patterns of Land Subsidence and Sinkhole Occurrence in the Konya Endorheic Basin. Turkey Geosci 14:5. https://doi.org/10.3390/geosciences14010005
Ozdemir A (2015) Investigation of sinkholes spatial distribution using the weights of evidence method and GIS in the vicinity of Karapinar (Konya, Turkey). Geomorphology 245:40–50. https://doi.org/10.1016/j.geomorph.2015.04.034
Öztürk MZ, Çetinkaya G, Aydın S (2017) Köppen-Geiger İklim Sınıflandırmasına Göre Türkiye'nin İklim Tipleri. J Geograp 35:17–27
Öztürk MZ, Şener MF, Şener M, Şimşek M (2018a) Structural controls on distribution of dolines on Mount Anamas (Taurus Mountains, Turkey). Geomorphology 317:107–116. https://doi.org/10.1016/j.geomorph.2018.05.023
Öztürk MZ, Şimşek M, Şener MF, Utlu M (2018b) GIS based analysis of doline density on Taurus Mountains. Turkey Environm Earth Sci 77:536. https://doi.org/10.1007/s12665-018-7717-7
Pekel J-F, Cottam A, Gorelick N, Belward AS (2016) High-resolution mapping of global surface water and its long-term changes. Nature 540:418–422. https://doi.org/10.1038/nature20584
Popovici EA, Bălteanu D, Kucsicsa G (2013) Assessment of changes in land-use and land-cover pattern in Romania using Corine Land Cover Database. Carpath J Earth Environm Sci 8:195–208
Raspini F, Caleca F, Del Soldato M et al (2022) Review of satellite radar interferometry for subsidence analysis. Earth Sci Rev 235:104239. https://doi.org/10.1016/j.earscirev.2022.104239
Roberts N (1983) Age, palaeoenvironments, and climatic significance of late Pleistocene Konya Lake, Turkey. Quatern Res 19:154–171. https://doi.org/10.1016/0033-5894(83)90002-9

Scheidt J, Lerche I, Paleologos E (2005) Environmental and economic risks from sinkholes in west-central Florida. Environ Geosci 12:207–217. https://doi.org/10.1306/eg.05130404009

Sevil J, Gutiérrez F (2023) Morphometry and evolution of sinkholes on the western shore of the Dead Sea. Implicat Suscept Assess Geomorphol 434:108732. https://doi.org/10.1016/j.geomorph.2023.108732

Sha T, Yao X, Wang Y, Tian Z (2022) A Quick Detection of Lake Area Changes and Hazard Assessment in the Qinghai-Tibet Plateau Based on GEE: A Case Study of Tuosu Lake. Front Earth Sci 10:934033. https://doi.org/10.3389/feart.2022.934033

Şĭrecĭ N, Aslan G, Çakir Z (2021) Long-term spatiotemporal evolution of land subsidence in Konya metropolitan area (Turkey) based on multisensor SAR data. Turkish J Earth Sci 30:681–697. https://doi.org/10.3906/yer-2104-22

Tanık A, Musaoğlu N, Altas L, et al (2018) Degradation of Ecological functions of Akgol Wetland in Turkey: effects and causes. In: 3rd International Conference Conference on Civil and Environmental Engineering (ICOCEE-2018). İzmir, pp 507–520

Taşoğlu E, Öztürk MZ, Yazıcı Ö (2024) High Resolution Köppen-Geiger Climate Zones of Türkiye. Intl J Climatol 44:5248–5265. https://doi.org/10.1002/joc.8635

Tudryn A, Motavalli-Anbaran S-H, Tucholka P et al (2021) Late Quaternary environmental changes of Lake Urmia basin (NW Iran) inferred from sedimentological and magnetic records. Quatern Int 589:83–94. https://doi.org/10.1016/j.quaint.2021.03.024

Ulu Ü (2009) 1/100.000 scale Turkish Geology Maps, Karaman M31 sheet.

Üstün A, Tusat E, Yalvac S (2010) Preliminary results of land subsidence monitoring project in Konya Closed Basin between 2006–2009 by means of GNSS observations. Nat Hazards Earth Syst Sci 10:1151–1157. https://doi.org/10.5194/nhess-10-1151-2010

Üstün A, Tuşat E, Yalvaç S et al (2015) Land subsidence in Konya Closed Basin and its spatio-temporal detection by GPS and DInSAR. Environ Earth Sci 73:6691–6703. https://doi.org/10.1007/s12665-014-3890-5

Vassileva M, Al-Halbouni D, Motagh M et al (2021) A decade-long silent ground subsidence hazard culminating in a metropolitan disaster in Maceió. Brazil Sci Rep 11:7704. https://doi.org/10.1038/s41598-021-87033-0

Vey S, Al-Halbouni D, Haghighi MH et al (2021) Delayed subsidence of the Dead Sea shore due to hydro-meteorological changes. Sci Rep 11:13518. https://doi.org/10.1038/s41598-021-91949-y

Waltham AC, Fookes PG (2003) Engineering classification of karst ground conditions. Q J Eng GeolHydrogeol 36:101–118

Weiss JR, Walters RJ, Morishita Y, et al (2020) High-Resolution Surface Velocities and Strain for Anatolia From Sentinel-1 InSAR and GNSS Data. Geophysical Research Letters 47:e2020GL087376. https://doi.org/10.1029/2020GL087376

Yao F, Livneh B, Rajagopalan B et al (2023) Satellites reveal widespread decline in global lake water storage. Science 380:743–749. https://doi.org/10.1126/science.abo2812

Yeşilmaden HM, İnan ÇA, Kurtuluş B et al (2021) Land subsidence assessment under excessive groundwater pumping using ESA Sentinel-1 satellite data: a case study of Konya Basin. Turkey Environ Earth Sci 80:409. https://doi.org/10.1007/s12665-021-09718-z

Yılmaz G, Çolak MA, Özgencil İK et al (2021) Decadal changes in size, salinity, waterbirds, and fish in lakes of the Konya Closed Basin, Turkey, associated with climate change and increasing water abstraction for agriculture. Inland Waters 11:538–555. https://doi.org/10.1080/20442041.2021.1924034

Yu C, Li Z, Penna NT, Crippa P (2018) Generic Atmospheric Correction Model for Interferometric Synthetic Aperture Radar Observations. JGR Solid Earth 123:9202–9222. https://doi.org/10.1029/2017JB015305